https://doi.org/10.5194/nhess-2023-73
Preprint. Discussion started: 8 June 2023

Natural Hazards and Earth System Sciences
Discussions

Prediction of landslide induced debris' severity using machine learning algorithms: a case of South Korea

Tuganishuri Jérémie[1], Chan-Young Yune[2], Gihong Kim[3], Seung Woo Lee[4], Manik Das Adhikari[5], Sang-GukYum[6*]

[1] Department of Civil and Environmental Engineering, Gangneung-Wonju National University, Gangneung, Gangwon-do, Republic of Korea, tugan.miya@gmail.com
[2] Department of Civil and Environmental Engineering, Gangneung-Wonju National University, Gangneung, Gangwon-do, Republic of Korea, yune@gwnu.ac.kr
[3] Department of Civil and Environmental Engineering, Gangneung-Wonju National University, Gangneung, Gangwon-do, Republic of Korea, ghkim@gwnu.ac.kr
[4] Department of Civil and Environmental Engineering, Gangneung-Wonju National University, Gangneung, Gangwon-do, Republic of Korea, swl@gwnu.ac.kr
[5] Department of Civil and Environmental Engineering, Gangneung-Wonju National University, Gangneung, Gangwon-do, Republic of Korea, rsgis.manik@gmail.com
[6] Department of Civil and Environmental Engineering, Gangneung-Wonju National University, Gangneung, Gangwon-do, Republic of Korea, skyeom0401@gwnu.ac.kr

[*]Corresponding author: Sang-Guk Yum; skyeom0401@gwnu.ac.kr

https://doi.org/10.5194/nhess-2023-73
Preprint. Discussion started: 8 June 2023

Natural Hazards and Earth System Sciences
Open Access
Discussions

Prediction of landslide induced debris' severity using machine learning algorithms: a case of South Korea

Abstract

Rainfall-induced landslides frequently occur in the mountainous region of Korean peninsula. The resulting landslide induced debris cause extreme property damages, huge financial losses and human deaths. To mitigate their effect different landslide susceptibility mapping are frequently used. However, these methods do identify regions with potential landslides but they do not quantify their severity. In this paper multi-category ordered machine models, namely, proportional odd logistic regression (POLR), random forest (RF), support vector machine (SVM), and extreme gradient boosting (EGB) methods, are proposed to fill the specified gap. Moreover, the exploratory data analysis on landslide induced derris's dataset has been conducted on to examine patterns and relationship between landslide-induced debris severity(size), causal factors(rainfall) and influencing factors. Findings revealed that cumulative three days' rainfall and slope length were most responsible for the severity of landslide-originated debris severity and slopes between 20° to 40° was identified as most vulnerable region. Furthermore, the predictive accuracy statistics were compared to assess the suitable model for debris severity for Korean case. The RF and EGB ranked higher with an overall accuracy of 90.07% and 86.09% and *kappa* of 0.72 and 0.61 on the validation set, respectively. The findings of this research may be useful in the identification of high risk zones for extreme rainfall-induced debris to elaborate mitigation and resilience policies, post-disaster rehabilitation planning and land use management.

Keywords: Rainfall-induced debris Severity; Proportional odd logistic regression; Random forest; Support vector machine; Extreme gradient boosting; Machine learning , South Korea

https://doi.org/10.5194/nhess-2023-73
Preprint. Discussion started: 8 June 2023

Natural Hazards and Earth System Sciences
Discussions

1. Introduction

Rainfall-induced debris is a natural phenomenon that occurs when the slope fails due to the saturation of soil after the rainfall exceeds a certain threshold (Au 1998; Takara et al. 2010; Peruccacci et al. 2017; Segoni et al. 2018; Crawford et al. 2019; Coppola et al. 2022). Rainwater penetrates the soil through cracks or pores (Zeng et al. 2022) which destabilizes the slope and induces landslides (Franzluebbers 2002). Furthermore, the volume of landslide-induced debris depends on the geological condition of the terrain, rainfall intensity and duration (Chang et al. 2011). Extreme rainfall is the triggering factor for landslides which is one of the most damaging natural disasters with the expensive cost of repair and indemnification (Kockelman 1986; Gariano and Guzzetti 2016). In addition, heavy windstorms, typhoons, and extensive rainfall have destroyed many properties and taken many human lives yearly (Liu et al. 2018). Furthermore, landslides have caused enormous environmental degradation, infrastructure damage, casualties, and loss of life, which disturb the socio-economic aspect of the community (Li et al. 2012; Sarkar and Dorji 2019; Zhao et al. 2019; Taylor et al. 2020; Lacroix et al. 2020; Winter 2020; Negi et al. 2020; Ju et al. 2020; Van et al. 2021). Most rainfall-induced landslides were found to be shallow (de Jesús et al. 2019; Liu et al. 2021; Chang et al. 2021) however, some were very extreme and resulted in severe human and financial damage (Turner, 2018; Meena et al., 2021). Klose et al. (2016) found that from 1980 to 2013, landslides took thousands of lives and an annual average of about $20 bilion of economic losses, which was 17% of the total ($121 billion) annual mean of global disaster-induced losses.

The Korean peninsula is characterized by mountainous, which makes it more prone to rainfall-induced landslides (Lee et al. 2013). Lee et al. (2012) found that the triggering factor for landslides was short-duration heavy rainfall. Park et al. (2013) reported that the annual property damage caused by rainfall-induced landslides in South Korea averaged between US$500M to US$1000M and approximately 36 human deaths per year from 1997 to 2010.

Therefore, to mitigate the effect of landslides in South Korea, different studies have been carried out on landslide assessment (Kadavi et al. 2019; Lee and Winter 2019; Sameen et al. 2020; Panahi et al. 2020; Hakim et al. 2022). Lee et al. (2020) applied the Naïve and Bayesian Networks model for landslide susceptibility mapping in Umyeon Mountain. Lee et al. (2012) used physical slope and probabilistic model, i.e., decision trees and logistic regression for landslide susceptibility mapping in Gangwon-do. Lee et al. (2013) developed the binary logistic regression model for predicting the occurrence of landslides. Woo et al. (2014) constructed a landslide hazard map using binary logistic regression. Park and Kim (2019) compared boosted trees and random forest model's performance in landslide susceptibility mapping for Umyeon Mountain; the same methods were previously applied at Pyeong-Chang by Kim et al. (2018). It was observed that the objectives of previous studies were to predict landslide susceptibility; they did not specify how severe the occurring landslides would be. Further, most of studies were performed on a small scale and only predicted the occurrence, not the size. Therefore, in the present study, we analyzed landslide-induced debris severity based on the causative variables and influencing factors. This study is novel in expressing the relationship of debris' severity, causative and influencing factors. It is an extention on landslide mapping which quantifies the magnitude of landslide-induced debris. The quantification of debris severity may be useful in land management by highlighting regions prone to higher rainfall-induced debris to know whether economic activities that may be carried out on the given region may not be vulnerable to extreme landslide hazards. The severity of debris is measured in unit of volume (m^3) and classified as shallow(below 500m^3) small(500-2000m^3), medium (2000-5000m^3) and critical, i.e., above 5000m^3. Words severity of debris, debris volume or size of debris express the same quantity in different ways and are used interchangeably in this manuscript.

https://doi.org/10.5194/nhess-2023-73
Preprint. Discussion started: 8 June 2023

2. Study region

Korean peninsula is located in the northern hemisphere, between China and Japan in Northeast Asia. Its climate has continental and oceanic features with wide temperature differences. The yearly mean temperature ranges from 10°C to 16°C, that is, from -6°C to 7°C in winter and 23°C to 27°C in summer. In South Korea, the rainy season range from June to September, with 1000mm to 1800mm of precipitation in the southern part and 1100 to 1400mm in the central region (https://web.kma.go.kr/).

The altitude ranges from 0 to 1911 meters, with mount Halla (in Jeju Island) being the highest peak in South Korea. The Gangwon Province is the most mountainous region of about 64% of all tallest mountains in Korea, that is, 23 of 36 mountains. The surface geology of the Korean peninsula is mostly composed of igneous, sedimentary, and metamorphic rock (Chough et al., 2000). The arable soil depth varies between 1 to 2m (Lee and Winter, 2019). Due to the high intensity rainfall and weak geological formation in the mountainous region causes high frequency of landslides. Figure 1(a) illustrates the distribution of landslides by the volume of landslides, while subplots (b & c) exhibited the relationship of slope length, altitude, and rainfall with the landslide size.

https://doi.org/10.5194/nhess-2023-73
Preprint. Discussion started: 8 June 2023

Natural Hazards and Earth System Sciences
Open Access
Discussions

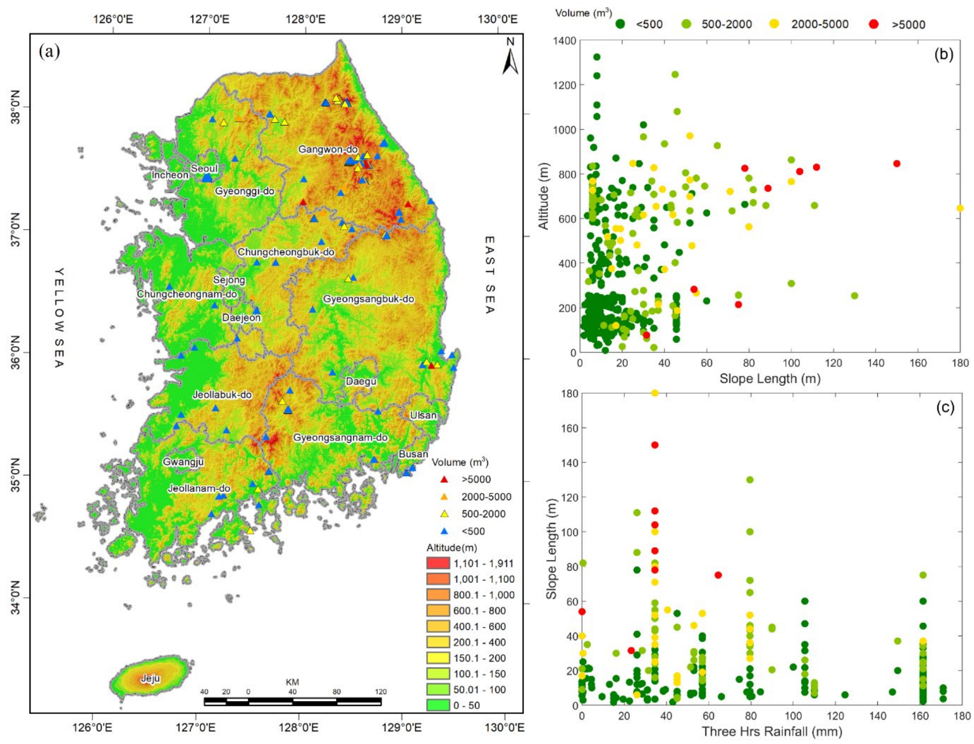

Figure 1. (a) Landslide location in South Korea, (b) Distribution of landslide volume per slope length and altitude, and (c) Distribution of landslide volume per slope length and rainfall (Data source: elevation data acquired from NGII, 2018).

3. Methodology

3.1. Problem formulation

Predictive models that deal with multi-variate random variables were investigated to predict the severity of rainfall-induced landslides. Among those predictive models, proportional odd logistic regression and other machine learning-based algorithms such as extreme gradient boosting, random forest, and support vector machine are widely used to deal with classification problems (Marjanović et al. 2011; Lee et al. 2012; Woo et al. 2014;Wang et al. 2022a). The main steps for the modeling process were to analyze the interaction of variables

https://doi.org/10.5194/nhess-2023-73
Preprint. Discussion started: 8 June 2023

that influence the severity of landslides with results in a higher size of debris. For the purposes, four machine learning models i.e., POLR, RF, SVM, and EGB, were used to assess the most suitable predictive model for landslide-induced debris in south Korea (;Su et al.,2022). The comparison was made using predictive accuracy and the value of *kappa*. Figure 2 shows the steps followed in the construction of the model.

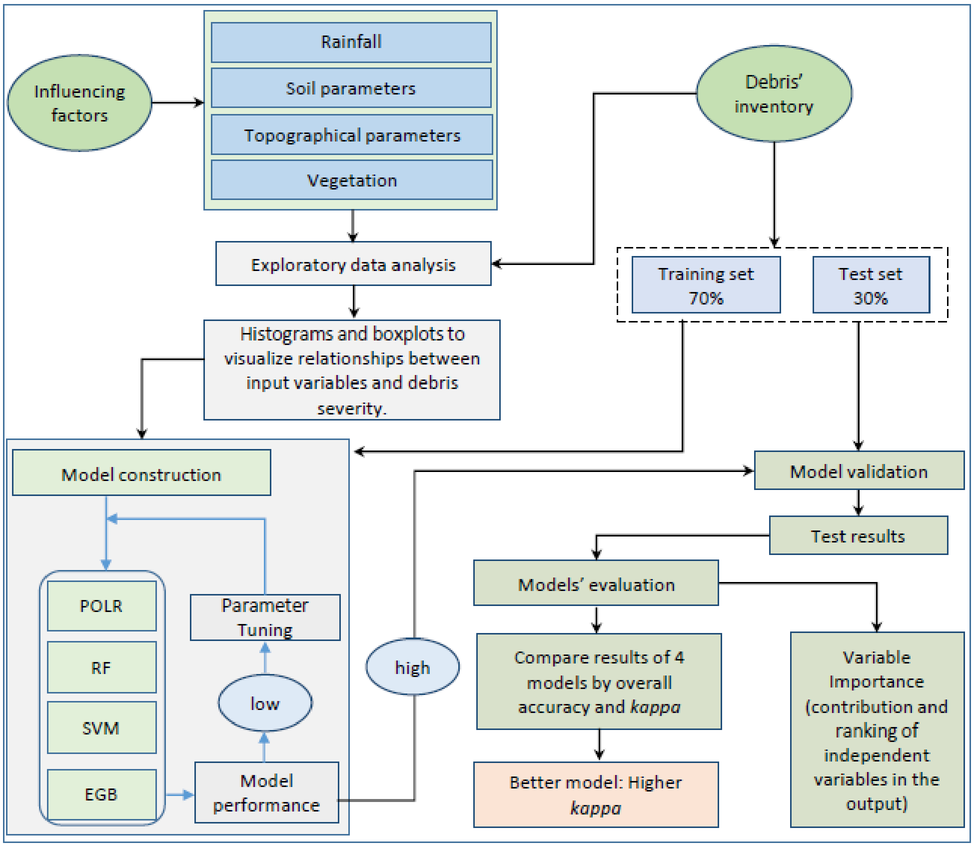

Figure 2. Modelling workflow process for the prediction of landslide induced debris' severity using machine learning algorithms.

3.2. Data description

The dataset contains 455 debris inventory collected from field surveys with the help of portable GPS, a laser ranger and a clinometer. Variable definitions and descriptions for each feature in the dataset are presented in Table 1. The rainfall data were collected from Korea meteorological Administration stations scattered around the country nearest each landslide-induced debris site. It was revealed that the duration and quantity of rainfall directly affect landslides (Berti et al. 2012; Kim et al. 2014; Sarkar et al. 2019; Liu et al. 2020; Ngo et al. 2021). Rainfall data were grouped into twelve variables: cumulative rainfall, continuous hourly rainfall, three hours, six hours, nine hours, twelve hours, one day, three days, seven days, two weeks, three weeks, and four weeks' rainfall. Different measures of rainfall were captured due to the time-dependent cumulative effect of rainfall on the slope stability, and prolonged rainfall has a more damaging effect in mountainous regions (Baum and Godt 2010; Hidalgo et al. 2017; Meena et al. 2022). The conditioning factors, i.e., soil type, topsoil depth, altitude, slope, slope-length, slope aspect, and vegetation (leafage, size of tree, age of trees, and fire history), were collected. The soil type was classified as sandy loam, lithosols, silt loam, and clay. The soil depth was grouped into below 20 centimeters, between 20-50, and 50-100 centimeters. The rainfall infiltrating the topsoil causes saturation, which initiates the landslide and then results in debris flow (Baum and Godt 2010;Vahedifard et al., 2017; Zhu and Zhang 2019). The anti-erosive drainage presence and status were categorized into: very good, good, and bad. Dranage channels reduces the concentration of water in soil and effect on water flow, saturation, soil moisture, and valley landslides(Shahabi and Hashim 2015). The vegetation-covered and necked lands have different affect of landslide (Lee et al. 2013; Ozioko and Igwe 2020;Huang et al. 2021). The foliage information was classified into pines, broad-leaved, and mixture, while, the size of trees was classified as large, small, and medium. The age of trees was grouped into seven classes viz. 1-5 5-15, 15-25, 25-35, 35-45 and >45 years. The forest fire history was also considered as a influencing factor due to its erosive nature(Huang et al. 2020). Geographical features were found to contribute to the severity of landslides at different levels; steep slopes

https://doi.org/10.5194/nhess-2023-73
Preprint. Discussion started: 8 June 2023

were found to fail as the intensity of the rainfall increased (Brand et al. 1984; Au 1998; Charles and Shi 1998; Nandi and Shakoor 2008; Pham et al. 2018; Chen et al. 2020). It was also noted that plane areas beneath steep slopes face the damage caused by debris flowing from the top of mountains (Raja et al. 2017,Wang et al. 2022b).

The output variable (volume) of landslides has been classified into four categories, i.e., below 500m^3, between 500-2000m^3, 2000-5000m^3, and above 5000m^3(Fig. 4c). There are different types of landslides; which are classified based on the cause or shape after occurrence (Causes 2001). Landslides may result from liquefaction, earthquakes, intense surface water flow due to precipitation, underground water, ice melting, human activities, tectonic movements etc.(Alexander 1992; Causes, 2001; van der Beek, 2021;McColl 2022). In this paper, we only considered landslide-induced debris originating from rainfall. Table 1 summarizes the characteristics of debris: its types, frequency and size.

Table 1: Landslide-induced debris types and frequency

Volume (m^3) / Destroyed area	<500	500-2000	2000-5000	>5000	Total
valley erosion	1	1	1		3
falling rocks	1				1
mixed/ complexes	3	2	1		6
slope	1	1		1	3
scour	1				1
curved wedges	4	1			5
a circular arc	205	45	14	2	266
Plane	120	35	10	5	170
Total	336	85	26	8	455

3.3 Exploratory data analysis

The relationship between the influencing factors and the debris size were analyzed. We consider categorical variables, also known as qualitative set of information, that is divided into groups. It describes data which are non-numerical and serve qualitative purposes, such as

https://doi.org/10.5194/nhess-2023-73
Preprint. Discussion started: 8 June 2023

representing a certain value or distinctive character of objects (nominal), when there is no order in levels and ordinal when there is an order in the dataset (Bilder and Loughin 2014). In addition, continuous features were presented in form of histograms and boxplots to analyze the dispersion and influence on the size of debris. Figure 3 illustrates that most of the occurred debris was shallow (below 500m^3, 73.85%), followed by 500-2000m^3 (18.68%), and the extreme debris (above 5000m^3) was the least frequent (1.76%). Debris with a size above 5000m^3 was mainly associated with sandy loam soil of depth above 20cm and a non-perfected drainage system, where the forest density was medium and in a place that experienced wildfire. The region with pines leafage experienced shallower debris compared to other types of leafage. The region with older trees, above 45 years of age, experienced more severe debris than younger forests. Šilhán and Stoffel (2015) highlighted that the area with timber age of above 45years were more sensitivity to landslide occurrences. The size of debris for wildfire-experienced regions was observable; compared to the frequency of cases with no wildfire history, the severity was quite higher. The wildfire influence on the rainfall-induced debris is due to the reduced infiltration of water into the soil, which increases the erodibility of soil (Ranger et al. 2020; Tiwari et al. 2020). The inadequate drainage system resulted in severe debris(Popescu 2002), where the system was very good, no severe debris occurred. The resulting huge number of shallow debris for a very good drainage system is due to the fact those systems are usually created in the most vulnerable regions and the shallow debris is an indication of improvement in landslide mitigation.

https://doi.org/10.5194/nhess-2023-73
Preprint. Discussion started: 8 June 2023

Natural Hazards and Earth System Sciences
Open Access
EGU
Discussions

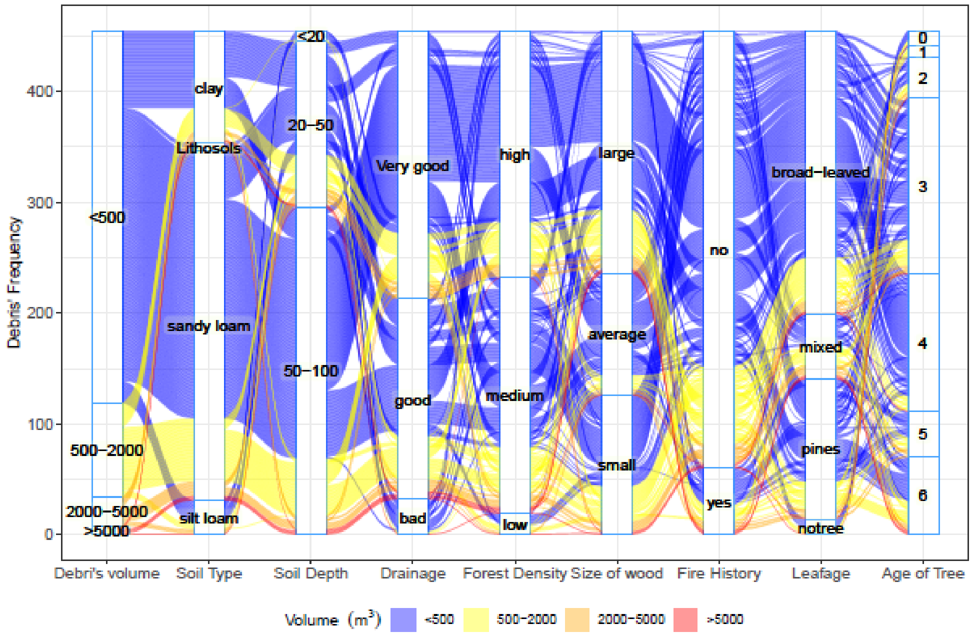

Figure 3. Interlinkage between the size of debris and categorical influencing factors.

Figure 4a illustrates that sandy soil, which totalizes about 70% of all debris, was the most vulnerable soil, followed by clay (22%), silt loam (7%) and lithosols (1%). Similarly, sandy soil not only ranked higher in terms of frequency but also in terms of size. The high sensitivity of sandy soil to rainfall-induced debris may be due to its high coefficient of permeability which facilitates fast saturation of topsoil during the rainfall period that induces shallow debris (Lee et al. 2013). Overall, about 73.85% of all debris was shallow, that is, below $500m^3$, 18.68 % ($500\text{-}2000m^3$) was small, 5.71% ($2000\text{-}5000m^3$) was medium, and only 1.76% were critical, i.e., above $5000m^{3,}$ as depicted in Fig. 4b. Figure 4c, illustrates that about 74% of landslide-induced debris occurred in Gangwon and Seoul; this made the two provinces more vulnerable than other regions. South and North Gyeongsang provinces ranked third and fourth with 7% (25 cases) and 5% (18 cases) of all debris inventory, respectively.

https://doi.org/10.5194/nhess-2023-73
Preprint. Discussion started: 8 June 2023

Natural Hazards and Earth System Sciences
Open Access
Discussions

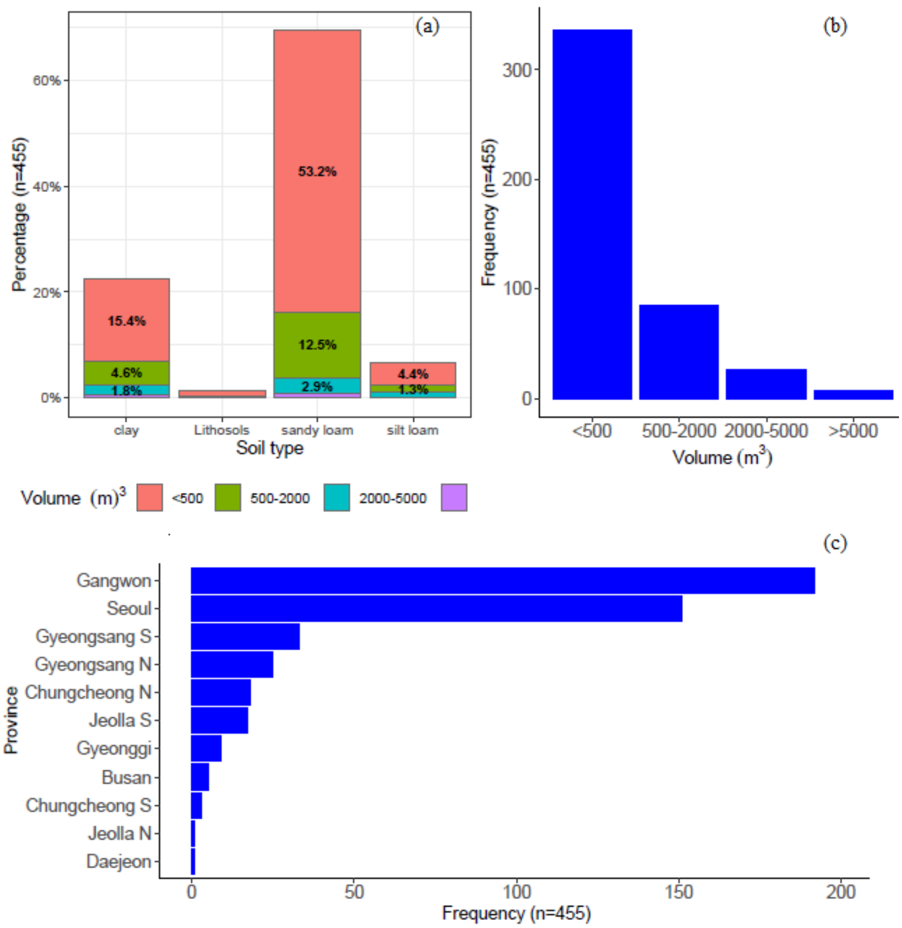

Figure 4. Distribution of debris': (a) debris' volume (in m^3) per soil types, (b) debris' frequency per volume, and (c) debris' frequency per provinces.

To examine the relationship between continuous explanatory variables and their effect on the size of debris, 3D scatter plots and boxplots were presented (Fig. 5). It was observed on the 3D scatterplot that most debris occurred at slope between 20° and 40° (Fig. 5a), this was also confirmed by the boxplot (Fig. 5b), where few exceptions were observed for shallow debris for clay and sandy soil where debris occurred at small or at very large slope angles as outliers. Shallow debris was independent of the slope angle as depicted in Fig.5c; outliers were

Natural Hazards and Earth System Sciences
Open Access
Discussions

scattered on all slope angles, and as the size of debris increased, the occurrence converged at slope between 20° and 40°. There was a pseudo-decreasing trend between altitude and size of debris (Fig. 5c), the highest altitudes (above 600m) were associated with shallow debris and critical debris occurred at altitude between 200 and 900m. On the other hand, a quasi-increasing relationship between size of debris and slope length was observed in all type of soil (Fig. 5d). Debris below 500m^3 was associated with slope length below 80m, the highest quartile was about 140m associated with clay soil of above 5000m^3 of debris size.

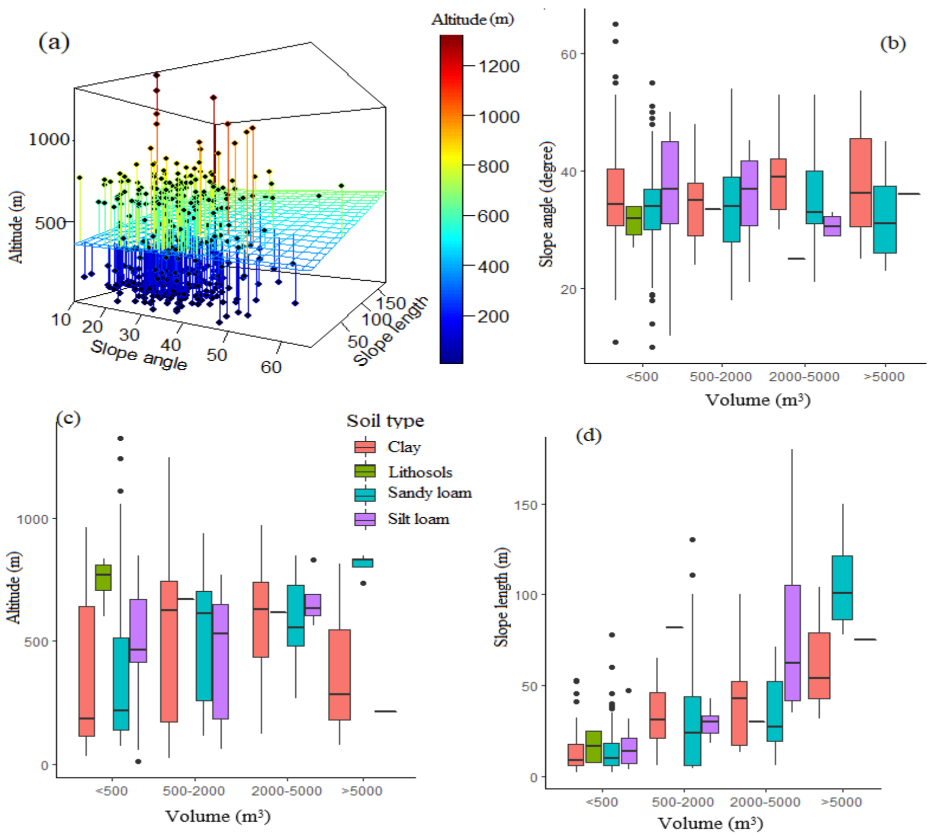

Figure 5. Distribution of debris and continuous predictors: (a) 3D Scatter plot between altitude, topographic slope and slope length, (b) boxplot of volume of debris per slope angle and soil types, (c) boxplot of volume of debris per altitude and soil types, and (d) boxplot of volume of debris per slope length and soil types.

https://doi.org/10.5194/nhess-2023-73
Preprint. Discussion started: 8 June 2023

The analysis of the relationship between the size of debris and rainfall over different time intervals has shown that short time rainfall was associated with shallow debris(fig.6 a-f), as the cumulative time interval of rainfall increased, the debris size increased and stabilized at three days cumulative rainfall(Fig. 6g). we observed that the increase in severity of debris was associated with lower precipitation as reflected in the yellow boxplot for debris above 5000m^3(Fig. 6. g-f), the precipitation of occurrence was below the corresponding median rainfall. Therefore the lower precipitation on prolonged time greater or equal to three days was responsible for severe debris. On the other hand, short-duration heavy rains were responsible for shallow debris(Polemio and Petrucci 2000).The relationship between shallow debris and heavy rain was reflected in the boxplot representing debris below 500m^3(Fig. 6 a-f), where the interquartile range of precipitation was large.

https://doi.org/10.5194/nhess-2023-73
Preprint. Discussion started: 8 June 2023

Natural Hazards and Earth System Sciences
Discussions

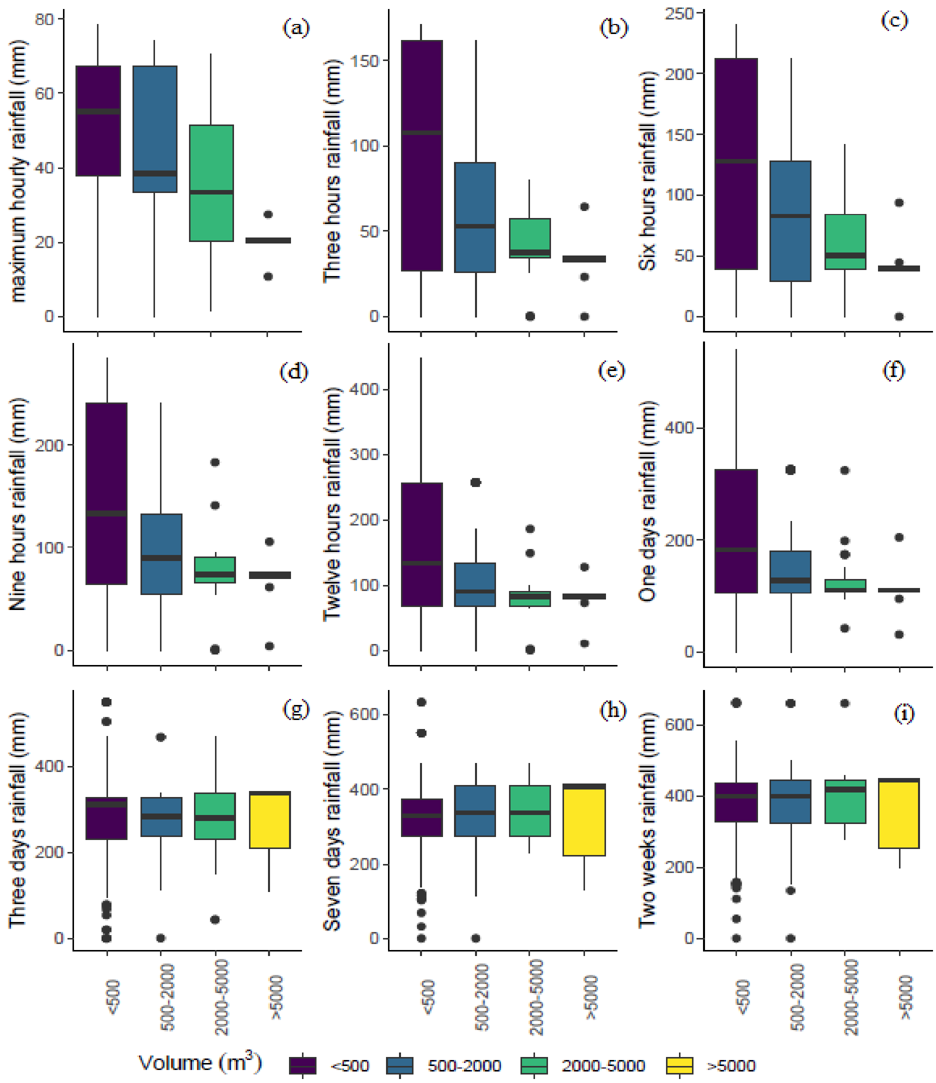

Figure 6. Distribution of severity of debris per antecedent rainfall groupped in different time intervals

The precipitation at the time of the incident exhibited an inverse relationship between the size of debris and rainfall intensity (Fig. 7 a-f). From three days' cumulative of antecedent rainfall, the relationship became almost constant in all time-based cumulative rainfall (Fig. 7 g-h). The rainfall of lower intensity falling over a prolonged period was observed to trigger the

https://doi.org/10.5194/nhess-2023-73
Preprint. Discussion started: 8 June 2023

large size of rainfall-induced debris (Tang et al. 2017; Rivas et al. 2022). The threshold for the triggering factor was the rainfall duration of atleast 3days (Chinkulkijniwat et al., 2020; Rahardjo et al., 2020). In terms of soiltype, clay exhibited shallow debris at lowest precipitation followed by sandy soil. The median of the occurrence of shallow debris was the lowest for silt loam compared with other soil types. From three days cumulative rainfall(Fig. 7g), the median of occurrence of all size of debris stabilized around 300mm of precipitation and clay was more likely to produce severe debris.

Natural Hazards and Earth System Sciences
Open Access
Discussions

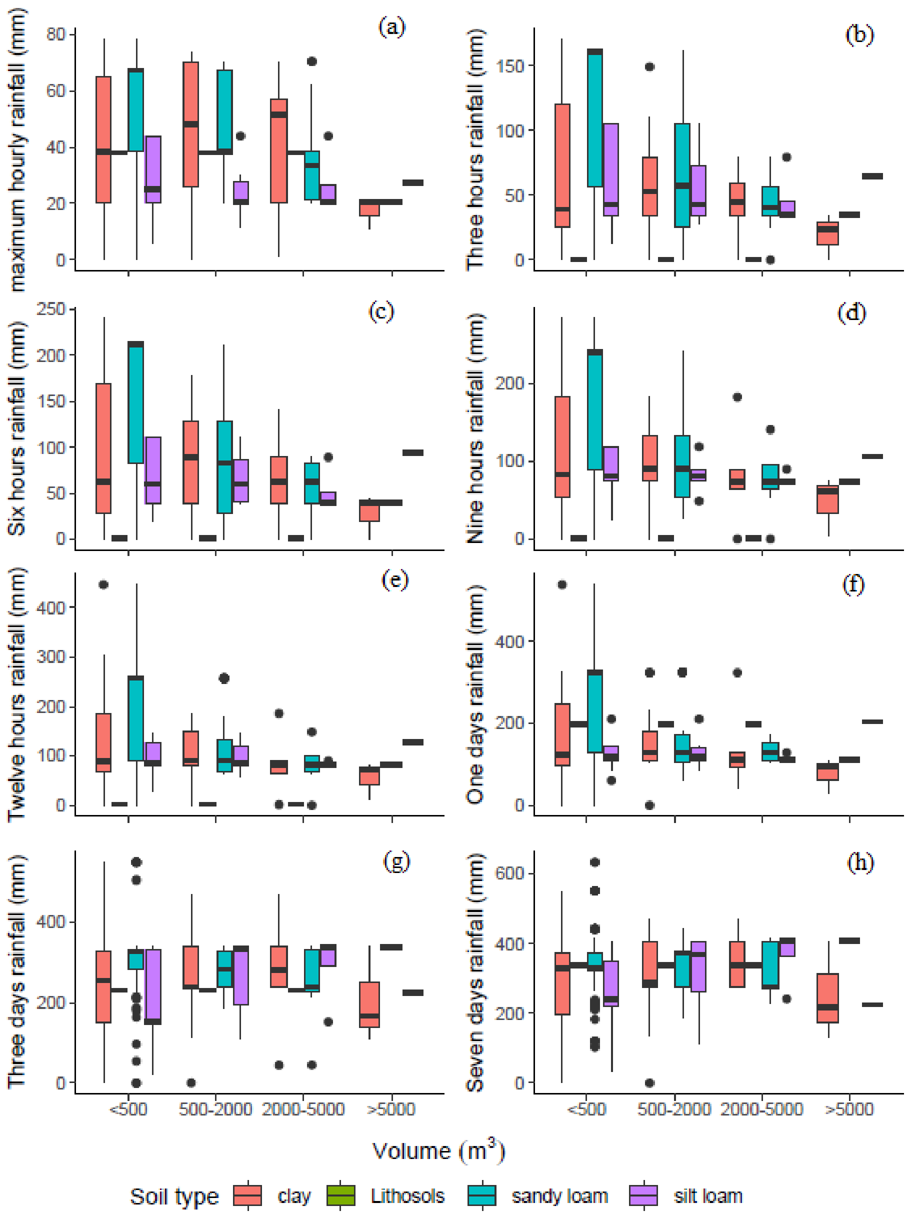

Figure 7. Relationship between rainfall and the size of debris.

3.3. Method Description

The analysis, construction, and evaluation of models were done in the following chronological order as depicted in Fig. 2. First, the data set was curated: formatting the variables to match their types, that is, numerical variables into a numerical format, and categorical variables into factor and ordered factors according to their natural characteristics (Table 1). Second, the dataset was split into training and test set. Third, the four machine learning algorithms (Kainthura and Sharma 2022; Su et al.,2022), were applied to the training and test set on all variables consecutively. Finally, confusion matrices for each method were generated to compare the performance based on the overall accuracy and *kappa*. The variable ranking plot was generated to identify the cause of differences in the predictive power of the four methods.

All analyses were done using the following packages in R software: Caret (Max 2022) for the creation of confusion matrix, dplyr (Wickham et al. 2022) for data manipulation and formatting, MASS for running proportional odd logistic model, Random Forest for running the random forest algorithm, Xgboost for running extreme gradient boost, SVM for supporting vector machine, Ggplot2 (Wickham 2016), alluvial (Brunson 2020) for plotting, and Matrix for creation of sparse matrix which is used in training extreme gradient boosting.

Variable importance is a systematic approach for identifying the contribution of input variable in the prediction of the outcome variable in the predicative model. For graphical representation of variable importance (Biecek and Burzykowski 2021), the plot was made using DALEX libraries (Biecek 2018) and the e1071 package (Meyer et al. 2021) in R (Team 2021). This plot ranks variables according to its influence on the predictive power of the model.

The selected methods for modeling were chosen based on low parsimony and are frequently applied to ordered outcome problems. The predictive performance for each model was evaluated using confusion matrix information accuracy and *kappa* (Caelen 2017). The

https://doi.org/10.5194/nhess-2023-73
Preprint. Discussion started: 8 June 2023

kappa statistic *k* measures the agreement between the observed and predicted values to quantify the ability of the model to classify the output variable into their appropriate classes or categories. Let both the observed Y variable and predicted Z variable have g categories or levels. Let f_{ij} be the frequencies of observations in the i^{th} categorical output variable Y and the j^{th} category of the predicted values, then the frequency table known as the confusion matrix can be arranged as follows:

$$
\begin{array}{lccccc}
 & Z=1 & Z=2 & \dots & Z=g \\
Y=1 & f_{11} & f_{21} & \cdots & f_{1g} \\
Y=2 & f_{21} & f_{22} & \cdots & f_{2g} \\
\vdots & \vdots & \vdots & \cdots & \vdots \\
Y=g & f_{g1} & f_{2g} & \cdots & f_{gg}
\end{array}
$$

The observed (actual values) ratio of agreement between Y and Z is expressed as:

$$p_0 = \frac{1}{n} \sum_{i=1}^{g} f_{ii} \quad (1)$$

and the expected agreement by chance is defined as:

$$p_e = \frac{1}{n^2} \sum_{i=1}^{g} f_{i+} f_{+i} \quad (2)$$

where f_{i+} is the total for the i^{th} row f_{i+} is the total for the i^{th} column. The value of kappa is the estimate of the population coefficient calculated using the following formula:

$$k = \frac{\Pr[Y=Z] - \Pr[y=z|Y \text{ and } Z \text{ are independent}]}{1 - \Pr[y=z|Y \text{ and } Z \text{ are independent}]} \quad (3)$$

https://doi.org/10.5194/nhess-2023-73
Preprint. Discussion started: 8 June 2023

The confusion matrix is useful for analyses, control tunes of different classifiers, and identification of a combination of classes with its recognition values or rates (Susmaga 2004). The confusion matrix is a (g × g) dimension table (matrix) which matches predicted values from the model vs. actual values from the dataset, where g stands for levels of the outcome variable, entries on the diagonal represents the correct classification, and non-diagonal elements represent misclassification. The accuracy is defined as the ratio of correctly classified entries and the sum of correctly classified and misclassification. The accuracy of the model is compared to the value of the No information rate (NIR). The NIR is the baseline for assessing performance, not 0.5. For the model to be useful (better than random guess), the lower bound for a 95% confidence interval (CI) of prediction must be greater than NIR (Garson 2021). The next paragraphs describe each method in detail.

The proportional odds logistic model (POLR) (McCullagh 1980) is one of the usefull methods designed to handle ordered or ranked outcome variables when the outcome categories (levels) are more than two. This model is constructed based on cumulative probability distribution (Brant 1990), $y_j = \Pr(y \leq j\ )$ and is expressed in the form:

$$\text{logit}\ [y_j/(1-y_j)] = \theta_j - \beta^t \text{X} \tag{4}$$

where y is a set of N and independent observation taking values j= 1, 2, …, k, X is a vector of independent variables, $\theta_1 < \theta_2 < \cdots < \theta_{k-1}$ and β^t are unknown parameters. To use ordinal regression, assumptions must be satisfied.

To use the proportional odds logistic regression, the proportional odd assumption or the parallel regression conditions must be satisfied. The first states that no independent variable has a disproportionate effect on any level of the dependent variable (McNulty 2021). If this condition is not satisfied, other methods such as adjacent logit models may be used (Agresti, 2010; Harrell, 2015). To test the parallel regression, the Brant-Wald test is used and this test

https://doi.org/10.5194/nhess-2023-73
Preprint. Discussion started: 8 June 2023

compares the general ordinal logistic regression (with no assumption of proportional odd) with POLR. It is the test of significance in the difference between the two models, which produces chi-square statistics. If the p-value of each of the different coefficients of variables in the model is greater than 0.05, then the parallel regression assumption holds (Brant 1990) or the assumption is violated otherwise. Binary logistic regression is frequentry used for landslide susceptiblity mapping(Yesilnacar and Topal 2005; Yilmaz 2009; Lin et al. 2017; Lombardo and Mai 2018; Sun et al. 2021), the ordered logistic regression is an extension for binary logistic applied to solve problems with multilevel ordered outcomes(Brant 1990).

The second used method was the Random Forest which is a classification and regression methods. The RF algorithm (Breiman 2001) is a combination of tree predictors and every tree is made based on values of random vectors, which are sampled independently using the same distribution to create all trees of the forest. In this study, the RF classification method (Biau and Scornet 2016; Lechner and Okasa 2020;) is appropriate due to its capability to handle multiple outcome-related problems (Diaz-Uriarte and de Andrés 2005). It was applied in different regions for landslide susceptibility mapping(He et al. 2021; Sun et al. 2021; Huang et al. 2022).

The third used method is SVM, which was widely used for mapping the likelihood of landslides (Lee et al., 2017). Among the multiple class prediction methods, the SVM method performed better for protein fold recognition (Ding and Dubchak 2001;Huang and Zhao 2018), landslide hazard (Hong et al. 2015), landslide spatial prediction (Pham et al. 2018), etc. SVM performed not only in multiclass problems but also better in ordered multilevel problems and it worked better than traditional regression methods (Li et al. 2012). More details about the SVM algorithm is described by Noble (2006).

The last but not least to choose was the EGB. Extreme gradient boosting is also a machine learning algorithm known for its high-speed performance and efficient prediction accuracy

https://doi.org/10.5194/nhess-2023-73
Preprint. Discussion started: 8 June 2023

(Chang et al. 2018). The algorithm is based on Friedman's work (Friedman 2001) and implemented in R under the package xgboost (Chen et al. 2015). This method is known for its high performance on larger sample sizes (Georganos et al. 2018).

4. Analysis & discussion

To identify the suitable model for the prediction of the size of debris, previously discussed methods were explored, and results were summarized and compared in this section.

4.1 Debris prediction using POLR

The significance of the observed relationship between the size of the debris and the associated explanatory variables was measured using proportional odd logistic regression. Variable selection was made using backward selection (Andersen 2010). The above coefficients can be interpreted as follows: taking into consideration of p-values, and for each case supposing that all other coefficients were held constant, the decrease in three hours' rainfall is associated with a 94% lower odd the size of debris, an increase is six hours' rainfall was associated with 4% increase in higher odd of the size of the debris (Table 2).

Table 2. POLR model coefficients.

Variables	Coefficient	P value	Odds ratio
Three hours rain	-0.051	<0.01	0.949
Six hours rain	0.039	<0.01	1.040
One day rain	-0.009	0.01	0.990
Slope length	0.039	<0.01	1.040
altitude	0.001	0.02	1.001
Drainage: Good	1.246	0.13	3.477
Drainage: Very good	1.818	0.04	6.164
Intercepts:			
<500|500-2000	2.313	<0.01	10.105
500-2000|2000-5000	4.455	<0.01	86.102
2000-5000|>5000	6.428	<0.01	619.397

https://doi.org/10.5194/nhess-2023-73
Preprint. Discussion started: 8 June 2023

The goodness of fit and model diagnostic result shows that McFadden pseudo-R^2 was 0.23 where the values between 0.2 and 0.4 indicated an excellent fit (Louviere et al. 2000). To test proportional odd assumptions, the Brant-Wald test (Brant, 1990) was used, and the result was summarized in Table 3. It shows that all probabilities for all variables including the omnibus are greater than the 0.05 threshold, except for slope length, which proves that the parallel regression assumption is satisfied.

Table 3. Parallel regression assumption test.

Test for	**X^2**	**df**	**Probability**
Omnibus	12.6	14	0.56
Three hours rain	1.76	2	0.41
Six hours rain	1.18	2	0.56
One day rain	1.18	2	0.55
Slope length	7.1	2	0.03
altitude	1.31	2	0.52
Drainage	0.19	4	1

The effect plot was used to demonstrate the change, in the likelihood of occurrence of landslides of a given volume, associated with the change in selected predictors. Figure 7 depicts the variation of probability of landslides of a given volume per three days' rainfall and slope length. The likelihood of occurrence of debris below 500m^3 was directly proportional to an increase in the rainfall for the slope length below 30m. There was a decrease in the occurrence of debris larger than 500m^3 as the rainfall increased. This decrease is an indication that shorter slope length was associated with a shallow debris (First column of Fig. 7). Moving from the first to the 4th column, the probability of shallow debris (below 500m^3), the probability shifted from 0.9 to 0.6 as slope length increased from 30m to 170m, and the long tail of probability plots for debris of size above 500m^3 disappeared as the slope-length and rainfall increased. This shifted up the probability curve for critical debris from 0.2 to 0.9 for slope length below 30m to 0.9 for slope length above 110m, respectively.

https://doi.org/10.5194/nhess-2023-73
Preprint. Discussion started: 8 June 2023

Natural Hazards and Earth System Sciences
Open Access
Discussions

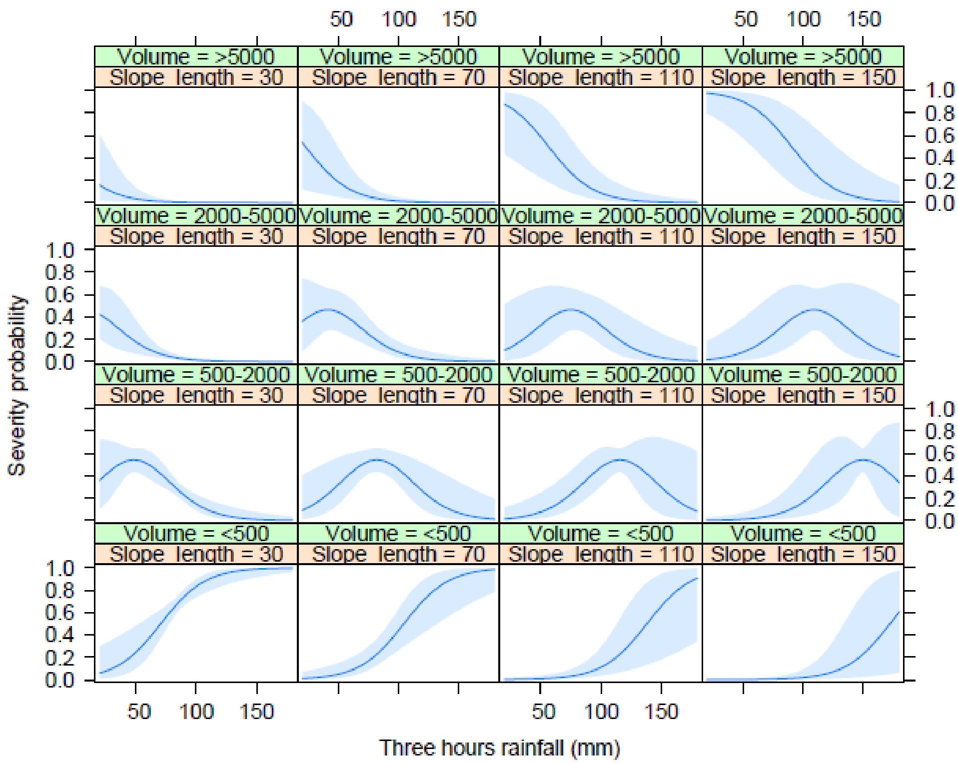

Figure 8. Effect of three hours of rainfall and slope length on size of debris.

Figure 9 illustrates that the maximum size of debris occurred at slope lengths above 50m and with rainfall between 80mm to 110mm. Looking at the two upper light hand corners of Fig. 9, the probability of occurrence of debris above 5000m^3 peaked at slope length above 100m and fade as the rain value increased, this fading associated with rain does not mean that there is an inverse relationship with rainfall but it associated with the rarity of heavy rain in the dataset. The probability of occurrence of shallow debris decreased as both altitude and slope length increased. On the other hand, the chance of occurrence of debris of size between 500m^3 and 2000m^3 increased with slope length and attained the maximum length between 70 and 80m with the maximum probability of occurrence of 0.6, and the last one decreased for slope length

https://doi.org/10.5194/nhess-2023-73
Preprint. Discussion started: 8 June 2023

above 100m. For the medeium sized debris, the maximum probability of occurrence was 0.7 and associated with slope lengths between 120m and 150m. The probability of occurrence of critical debris increased exponentially with slope length and altitude.

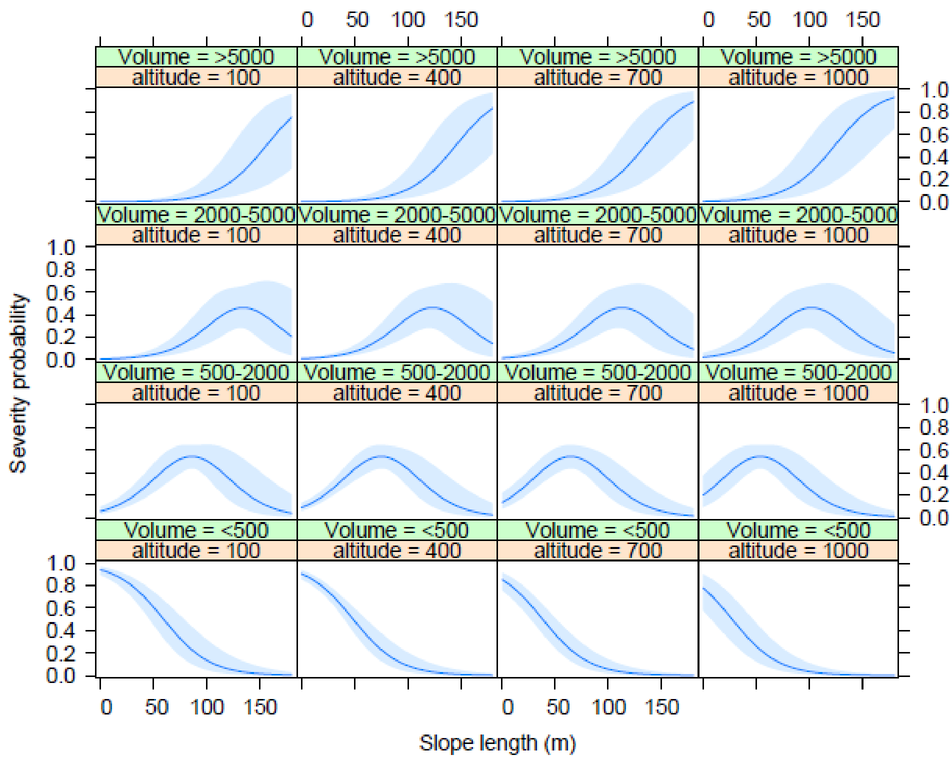

Figure 9. Effect of altitude and slope length on size of debris.

The intuitive explanation of the continuous decrease with shallow debris is associated with the cumulative character of the model, which means that, what looks like a decrease is not a real decrease, it is a shift from a lower level to a higher level associated with an increase in variables into consideration. For altitude below 300m, shifting from a size below 500m^3 to 500-2000m^3 happened at 20m of slope length, while shifting from 500-2000m^3 to 2000-5000m^3 and above occurred at slope length between 60 to 80m.

https://doi.org/10.5194/nhess-2023-73
Preprint. Discussion started: 8 June 2023

4.2 Debris prediction using RF

The random forest model was run on the training set of 304 observations. The number of grown trees was 1000, the variable tried at each split was 4, and the out-of-bag error estimates (OOB) error rate was 24.42%. Figure 10a depicts the predictions of a class below 500m^3 that had the least errors. Since the model is for classification, to calculate the prediction error, the model was run on the test set. The variable importance graph illustrates the slope length was the most contributing variable to the model accuracy (Fig. 10b). The mean decrease Gini (cross-entropy loss after permutation) value is the measure of the contribution of each variable to the homogeneity of nodes and leaves in the random forest (Martinez-Taboada and Redondo 2020). The higher the value, the more important the variable is, which exhibited that slope length is more influencing factor for the size of debris.

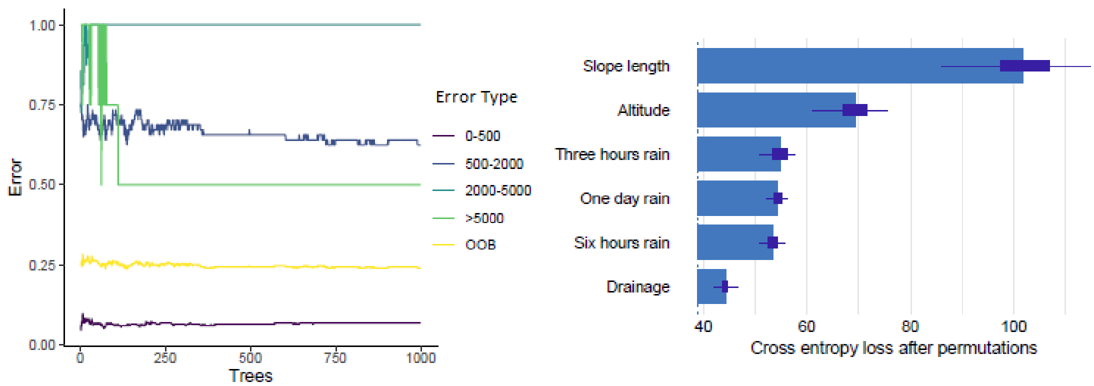

Figure 10. RF model: (a) training error rate, and (b) variable importance.

4.3 Debris prediction using EGB

To run the EGB, the train and test set were transformed into a sparse matrix, as it is run on numerical data matrices (Chen et al. 2022). The optimum model was obtained at the 881 number of iterations and the learning rate of 0.3. Since the task was a multi-classification, the multi: softmax objective was used (Chen et al. 2022). The evaluation metric was mlogloss

https://doi.org/10.5194/nhess-2023-73
Preprint. Discussion started: 8 June 2023

(Multi-class log loss) (Kabani and El-Sakka 2016). While training the model, the minimum mlogloss were 0.025 and 0.088 for the training and test sets respectively (Fig. 11a). The difference between training and the test error is due to the larger variance associated with the fewer number of observations in the test set. The extreme gradient boosting associated with higher importance to slope length, altitude, slope and three hours of rainfall, respectively (Fig. 11b).

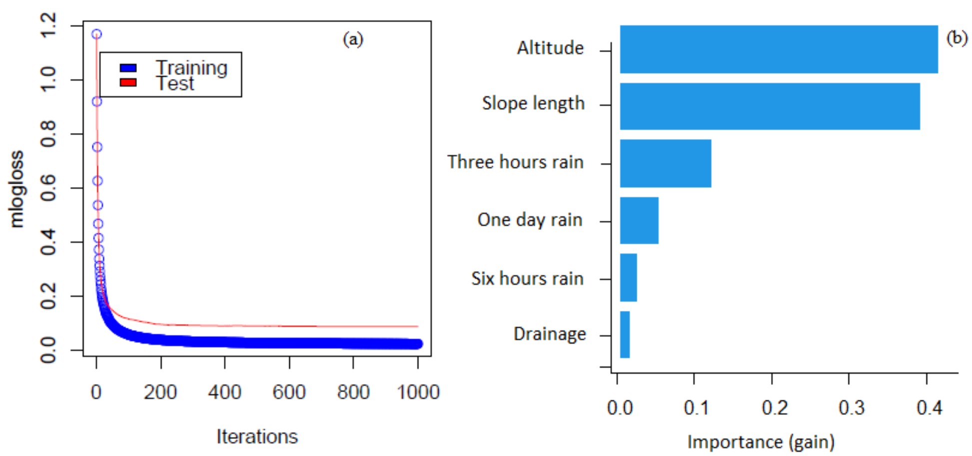

Figure 11. EGB model: (a) error rate and (b) variable importance.

4.4 Debris prediction using SVM

The support vector classification model with linear kernel was applied, and the number of support vectors was 142. The outcome of SVM model shown a higher performance rate on the test than the training set. Figure 11a depicts a two-dimensional projection of train data using slope length and three hours of rainfall showing different shading and support vectors. One of the weaknesses of the SVM, it classified predictions into two lower classes as indicated in Fig. 12a, it couldn’t distinguish the moderates from extreme debris. The SVM assigned higher importance to slope length and three hours of rainfall as the second high ranking variable as

https://doi.org/10.5194/nhess-2023-73
Preprint. Discussion started: 8 June 2023

shown in Fig. 11b.

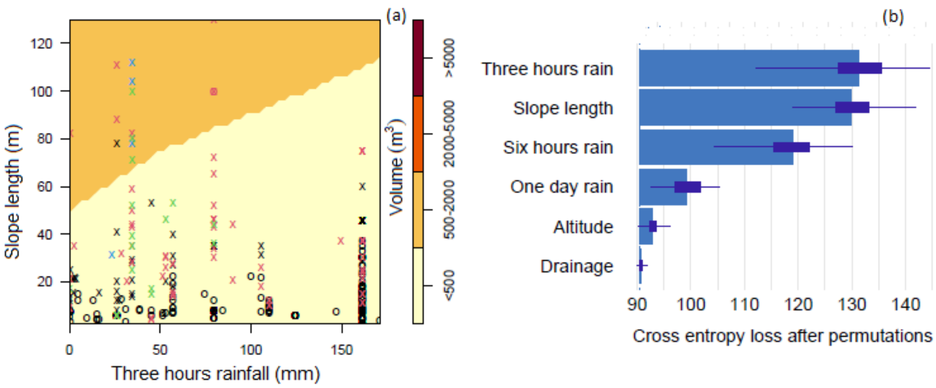

Figure 12. SVM model: (a) SVM classification plot, and (b) variable importance.

4.4 Discussion and model suitability assessment for landslide-induced debris severity prediction

This study analyzed the relationship between the severity of landslide-induced debris. The exploratory data analysis revealed that 93% of occurred debris was below 2000m^3. The Gangwon province and Seoul were more vulnerable regions in terms of the frequency of incidents. Despite a higher frequency of debris in Seoul, their size was small compared to Gangwon province with higher number of cases and more large sized-debris. To analyse the significance of the relationship between the size of debris with different models ranked the slope length as the most influential variable for the size of the debris. To visualize the association of the slope lengh with the size of debris, the scatter plot (Fig.13) revealed that the pattern of increasing trend of slope length and size of debris was more remarkable across all provinces, shallow debris were associatted with slope length blow 50m. The debris cases were clustered between 20° and 40°, as depicted in Fig.13, and critical debris tended to be clustered around 30 degrees; the association of slope angle and size of debris was not statistically significant. For the soil-debris size relationship, sandy soil and clay were associated with a

https://doi.org/10.5194/nhess-2023-73
Preprint. Discussion started: 8 June 2023

Natural Hazards and Earth System Sciences Open Access Discussions

higher frequency of debris; they exhibited shallow debris in all provinces except in Gangwon where severe debris occurred. It was observed that even though the silt loam soil was not highly frequent, it was vulnerable to severe debris as the slope length increased. Gangwon province was the region where the increasing relationship between the size of debris was observed, other provinces were not prone to severe debris.

https://doi.org/10.5194/nhess-2023-73
Preprint. Discussion started: 8 June 2023

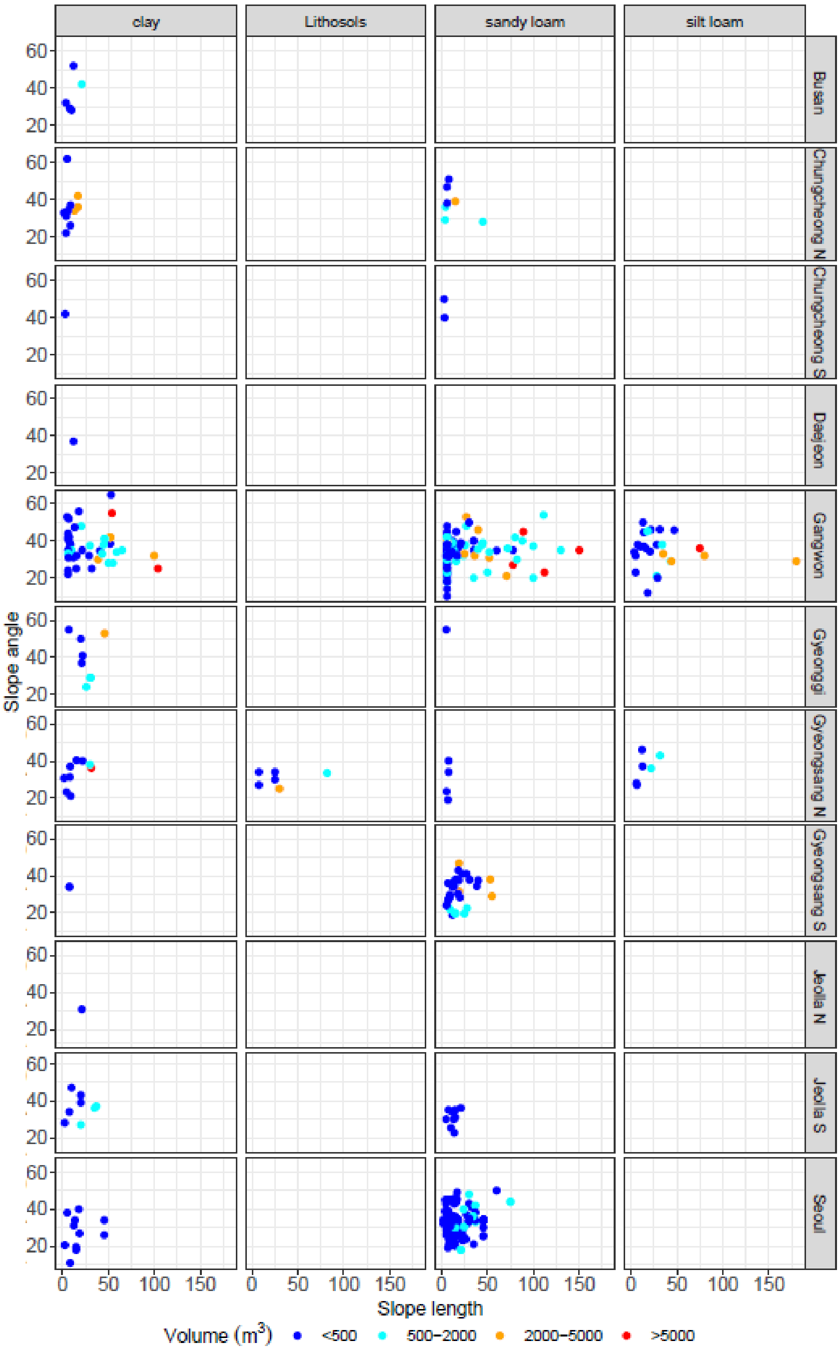

473

474 Figure 13. Province-wise scatter plot of debris' size per slope length, slope angle and soil

types.

To assess the suitability of utilized models, it was observed that the ordinal regression prediction power was low due to its inherent weakness; it does not perform well on the imbalanced dataset (Agresti 2010). That is, the outcome variable has some more prevalent levels than others. It also estimates the coefficient using maximum likelihood techniques, which require a large sample size, the used dataset was highly imbal anced. Figure 7 revealed that almost 80% of all occurred debris was shallow, as result, the model coefficients became unstable with larger prediction intervals. Despite the weakness, the ordinal model has the effect display (Fox and Weisberg 2019), which clearly shows the effect of each variable to each extent and the associated probability. The predictive performance for each of the four discussed methods was summarized in Table 4 to facilitate their comparison. The random forest model performed well in all cases on the training set and validation as well. This model associated the influencing factor with higher importance and lower importance to rain-associated variables. RF prediction accuracy was very high on the training set (0.93), and 0.90 on the test set. The prediction at 95% of confidence interval width ranged from 0.84 to 0.94 on training and test sets, respectively. The NIR shifted from 72.28% to 74.17%, and this small increase is due to a small sample of the validation set.

The model accuracy for POLR was quite moderate based on the *kappa* value of 0.38. The performance accuracy was better, the no information rate, NIR=0.7228<0.7314 lower boundaries of CI on the training set. This last condition was not satisfied for the test set, that is NIR=0.74 was higher than 0.69, which was the lower CI for the prediction interval on the test set. Based on the p-value for the prediction on test 0.26 > 0.05, the performance was not reliable. This is confirmed by the overall performance metric *kappa* =0.30, which was quite moderate.

https://doi.org/10.5194/nhess-2023-73
Preprint. Discussion started: 8 June 2023

The EGB model ranked the second best model after the RF, it satisfied all prediction conditions the overall performance (*kappa* = 0.6121) was slightly below the random forest 0.7273. The SVM model result was satisfactory for the training set. The lower bound of very close to the information rate and the overall performance was moderate (*kappa*=0.32), the weakness of the model was its incapacity to distinguish the moderate debris from the extreme ones; as result, it predicted all debris into two lower categories in Fig. 8a. The NIR fell into the prediction interval on the validation set, and the p-value was 0.11>0.05, which is an indication of moderate prediction accuracy.

Table 4. Model accuracy statistics for the four methods.

		Model accuracy statistics				
Method	**Data**	**Accuracy**	**95% CI**	**NIR**	**P-Value**	***kappa***
	Train	0.93	(0.89, 0.95)	0.72	<0.001	0.82
RF	Test	0.90	(0.84, 0.94)	0.74	<0.001	0.72
	Train	0.78	(0.73, 0.82)	0.72	0.011	0.38
POLR	Test	0.76	(0.69, 0.83)	0.74	0.26	0.3
	Train	0.77	(0.72, 0.82)	0.72	0.015	0.32
SVM	Test	0.78	(0.71, 0.85)	0.74	0.11	0.3
	Train	0.86	(0.81, 0.89)	0.72	<0.001	0.63
EGB	Test	0.86	(0.79, 0.91)	0.74	0	0.6

The landslide-induced debris prediction is an extension of landslide susceptibility mapping and may be useful in the quantification and prediction of debris resulting from a rainfall-induced landslide. This quantification can facilitate risk management (Ho and Ko 2009), in the identification of regions prone to severe debris and the making of policies for mitigation (Carmela and Mario Parise 2022). For example the decision of planting more vegetation that fits the conditions of the region to strengthen the soil or deciding an appropriate activity to be done in a given region to improve stability ,safety and efficient land use (Mayer et al. 2008) . Furthermore, some activities in regions prone to severe debris may be prohibited for the safety and well-being of the public(Frattini et al. 2010; DeGraff and Romesburg 2020; Di Napoli et al. 2020). In addition, the model may serve the disaster manager to create appropriate funds for post-disaster recovery. For example, if a region is expected to have shallow debris, the manager may establish a small fund for paying minor labour to repair the damaged environment. In extreme cases, a big fund may be created to pay for machinery and construction of preventive walls, plantation, and cost of machinery to remove debris in the affected region, to rehabilitate the impacted economic activities in the neighbourhood (Kachi et al. 2016). Due to the lack of financial data associated with the inventories the cost of post-disaster recovery was not estimated, more studies in the future may be carried out to fill this gap. The approach in this paper is valid for the studied area based on the user input data; more research in the future may be conducted to know whether the findings in this paper are general for regions with different characteristics or settings.

6. Conclusions

The study analyzed the relationship between the size of rainfall-induced debris and causal factors, i.e., time-based cumulative rainfall and influencing factors: soil types, vegetation, and geomorphology features. The exploratory data analysis revealed that the Gangwon province is prone to more frequent and more severe landslide-induced debris. Soil-related information revealed that the landslide-induced debris was more frequent in sandy soil and more severe, but its influence was not statistically significant in the predictive model. The region with non-perfected drainage systems also experienced severe debris. The regions with old timber that experienced fire had a higher debris likelihood. To examine the significance and to identify the suitable model for landslide-induced debris severity, four predictive modeling techniques i.e., POLR, RF, EGB and SVM, were applied to examine the causal and influencing factors of the severity of rainfall-induced debris in South Korea. The performance metrics, accuracy and

https://doi.org/10.5194/nhess-2023-73
Preprint. Discussion started: 8 June 2023

kappa were applied to compare the predictive power of each of the four methods. The findings of this research revealed that three hours' rainfall, one-day rainfall, and slope length were the most influencing factor and altitude took the second place. This finding was consistent with the results of Lee et al. (2012), stating that short-duration rainfalls were responsible for landslides and are the cause of their severity. The comparative analysis has shown that random forest had better predictive power with an accuracy of 90% and *kappa* = 0.72, and extreme gradient boosting followed with an accuracy of 86% (*kappa* = 0.6). The last two methods SVM with an accuracy of 78% (4% above NIR), and POLR performance was moderate at 76%, which is only 2% above 74% performance decision basis (No information rate NIR), but we did not have enough information to confirm their use as a basis for creation early warning system for rainfall-induced extreme debris. This is because POLR does not perform well on limited and imbalanced data (Rahman et al. 2021), which is the root cause of a wide range of prediction intervals. Thus, RF and EGB may be used as a suitable models for rainfall-induced debris prediction. The creation of a nationwide landslide database would solve the shortage of reliable data and allow the usage of more alternative methods, which will result in more improved models. The findings of this research may be used for the elaboration of rainfall-induced debris mitigation policies such as post-disaster rehabilitation planning and land use management.

List of abbreviations

- DALEX: moDel Agnostic Language for Exploration and explanation.
- MASS: Modern Applied Statistics with S.
- SVM: Support Vector Machine.
- POLR: Proportional Odd Logistic Regression.
- EGB: Extreme Gradient Boosting.
- RF: Random Forest.

- NIR: No information Rate.
- Acc: Accuracy.
- CI: confidence interval.
- OOB: Out Of Bag error estimates.
- CFM: Confusion Matrix.
- Caret: Classification and Regression Training

Acknowledgments:

This research was supported by Basic Science Research Program through the National Research Foundation of Korea (NRF) funded by the Ministry of Education (2021R1A6A1A03044326), and the grant (NRF-2021R1C1C2003316) funded by the National Research Foundation of Korea (NRF).

Data availability:

The datasets used and/or analyzed during the current study are available from the corresponding author on reasonable request.

Declaration of Competing Interest:

The authors declare that there are no conflicts of interest.

https://doi.org/10.5194/nhess-2023-73
Preprint. Discussion started: 8 June 2023

References

Agresti, A., 2010. Analysis of ordinal categorical data (Vol. 656). John Wiley & Sons.

Alexander, D.,1992. On the causes of landslides: Human activities, perception, and natural processes. Environmental Geology and Water Sciences, 20(3), 165-179.

Andersen, C. M., Bro, R., 2010. Variable selection in regression a tutorial. Journal of chemometrics, 24(11-12), 728-737.

Au, S. W. C., 1998. Rain-induced slope instability in Hong Kong. Engineering Geology, 51(1), 1-36.

Baum, R. L., Godt, J. W., 2010. Early warning of rainfall-induced shallow landslides and debris flows in the USA. Landslides, 7(3), 259-272.

Berti, M., Martina, M. L. V., Franceschini, S., Pignone, S., Simoni, A., Pizziolo M., 2012. Probabilistic rainfall thresholds for landslide occurrence using a Bayesian approach. Journal of Geophysical Research: Earth Surface, 117(F4).

Biau, G., Scornet, E., 2016. A random forest-guided tour. Test, 25(2), 197-227.

Biecek P., 2018. DALEX: Explainers for Complex Predictive Models in R. Journal of Machine Learning Research, 19(84), 1-5. https://jmlr.org/papers/v19/18-416.html

Biecek, P., Burzykowski, T., 2021. Explanatory model analysis: Explore, explain and examine predictive models. Chapman and Hall/CRC.

Bilder, C. R., Loughin, T. M., 2014. Analysis of categorical data with R. CRC Press.

Brand, E. W., Premchitt, J. E. R. A. S. A. K., Phillipson, H. B., 1984, September. Relationship between rainfall and landslides in Hong Kong. In Proceedings of the 4th International Symposium on Landslides (Vol. 1, No. 01, pp. 276-84). Toronto: Canadian Geotechnical Society.

Brant, R., 1990. Assessing proportionality in the proportional odds model for ordinal logistic regression. Biometrics, 46, 1171–1178.

Breiman, L., 2001. Random forests. Machine learning, 45(1), 5-32.

Brunson, J. C., 2020. ggalluvial: Layered, Grammar for Alluvial Plots. Journal of Open Source Software, 5(49), doi:10.21105/joss.02017. <https://doi.org/10.21105/joss.02017>.

Caelen, O., 2017. A Bayesian interpretation of the confusion matrix. Annals of Mathematics and Artificial Intelligence, 81(3), 429-450.

Carmela and Mario Parise 2022. A Chronological Database about Natural and Anthropogenic Sinkholes in Italy. Geosciences 12:5, pages 200

Causes, L., 2001. Landslide types and processes. US Geological Survey: Reston, VA, USA.

Chang, C. W., Lin, P. S., Tsai, C. L., (2011). Estimation of sediment volume of debris flow caused by extreme rainfall in Taiwan. Engineering Geology, 123(1-2), 83-90.

Chang, W. J., Chou, S. H., Huang, H. P., Chao, C. Y., (2021). Development and verification of coupled hydro-mechanical analysis for rainfall-induced shallow landslides. Engineering Geology, 293, 106337.

Chang, Y. C., Chang, K. H., Wu, G. J., 2018. Application of eXtreme gradient boosting trees in the construction of credit risk assessment models for financial institutions. Applied Soft Computing, 73, 914-920.

Charles W. W., Shi, Q., 1998. A numerical investigation of the stability of unsaturated soil slopes subjected to transient seepage. Computers and Geotechnics, 22(1), 1-28.

Chen, T., He, T., Benesty, M., Khotilovich, V., Tang, Y., Cho, H., Chen, K., Mitchell, R., Cano, I., Zhou, T., Li, M., Xie, J., Lin, M., Geng, Y., Li, Y., Yuan, J., 2022. xgboost: Extreme Gradient Boosting. R package version 1.6.0.1 https://CRAN.R project.org/package=xgboost

Chen, T., He, T., Benesty, M., Khotilovich, V., Tang, Y., Cho, H., Chen, K., 2015. Xgboost: an extreme gradient boosting. R package version 0.4-2, 1(4), 1-4.

Chen, Y., Withanage, K. R., Uchimura, T., Mao, W., Nie, W., 2020. Shear deformation and

https://doi.org/10.5194/nhess-2023-73
Preprint. Discussion started: 8 June 2023

failure of unsaturated sandy soils in surface layers of slopes during rainwater infiltration. Measurement, 149, 107001.

Chinkulkijniwat, A., Salee, R., Horpibulsuk, S., Arulrajah, A., & Hoy, M. (2022). Landslide rainfall threshold for landslide warning in Northern Thailand. Geomatics, Natural Hazards and Risk, 13(1), 2425-2441.

Chough, S. K., Kwon, S. T., Ree, J. H., Choi, D. K., 2000. Tectonic and sedimentary evolution of the Korean peninsula: a review and new view. Earth-Science Reviews, 52(1-3), 175-235.

Coppola, L., Reder, A., Tarantino, A., Mannara, G., Pagano, L., 2022. Pre-failure suction-induced deformation to inform early warning of shallow landslides: Proof of concept at slope model scale. Engineering Geology, 106834.

Crawford, M. M., Bryson, L. S., Woolery, E. W., Wang, Z., 2019. Long-term landslide monitoring using soil-water relationships and electrical data to estimate suction stress. Engineering Geology, 251, 146-157.

Dahal, R. K., Hasegawa, S., Nonomura, A., Yamanaka, M., Masuda, T., Nishino, K., 2008. GIS-based weights-of-evidence modeling of rainfall-induced landslides in small catchments for landslide susceptibility mapping. Environmental Geology, 54(2), 311-324.

de Jesús Arce-Mojica, T., Nehren, U., Sudmeier-Rieux, K., Miranda, P. J., Anhuf, D., 2019. Nature-based solutions (NbS) for reducing the risk of shallow landslides: where do we stand? International journal of disaster risk reduction, 41, 101293.

DeGraff, J. V.,and Romesburg, H. C. 2020. Regional landslide—susceptibility assessment for wildland management: a matrix approach. In Thresholds in geomorphology (pp. 401-414). Routledge.

Di Napoli, M., Carotenuto, F., Cevasco, A., Confuorto, P., Di Martire, D., Firpo, M., ...and

https://doi.org/10.5194/nhess-2023-73
Preprint. Discussion started: 8 June 2023

Calcaterra, D. 2020. Machine learning ensemble modelling as a tool to improve landslide susceptibility mapping reliability. Landslides, 17(8), 1897-1914.

Diaz-Uriarte, R., de Andrés, S. A., 2005. Variable selection from random forests: application to gene expression data. arXiv preprint q-bio/0503025.

Ding, C. H., Dubchak, I., 2001. Multi-class protein fold recognition using support vector machines and neural networks. Bioinformatics, 17(4), 349-358.

Fox, J., Weisberg, S., 2019. An R companion to applied regression 3rd ed Sage Thousand Oaks.

Franzluebbers, A. J., 2002. Water infiltration and soil structure related to organic matter and its stratification with depth. Soil and Tillage research, 66(2), 197-205.

Frattini, P., Crosta, G.,and Carrara, A. 2010. Techniques for evaluating the performance of landslide susceptibility models. Engineering geology, 111(1-4), 62-72.

Friedman, J. H., 2001. Greedy function approximation: a gradient boosting machine. Annals of Statistics, 1189-1232.

Gariano, S. L., Guzzetti, F. 2016. Landslides in a changing climate. Earth-Science Reviews, 162, 227-252.

Garson, G., 2021. Data Analytics for the Social Sciences: Applications in R. 10.4324/9781003109396.

Georganos, S., Grippa, T., Vanhuysse, S., Lennert, M., Shimoni, M., Wolff, E., 2018. Very high-resolution object-based land use–land cover urban classification using extreme gradient boosting. IEEE geoscience and remote sensing letters, 15(4), 607-611.

Hakim, W. L., Rezaie, F., Nur, A. S., Panahi, M., Khosravi, K., Lee, C. W., Lee, S., 2022. Convolutional neural network (CNN) with metaheuristic optimization algorithms for landslide susceptibility mapping in Icheon, South Korea. Journal of environmental management, 305, 114367.

Harrell, F. E., 2015. Ordinal logistic regression. In Regression modeling strategies (pp. 311-

https://doi.org/10.5194/nhess-2023-73
Preprint. Discussion started: 8 June 2023

325). Springer, Cham.

He, Q., Wang, M. and Liu, K.,2021. Rapidly assessing earthquake-induced landslide susceptibility on a global scale using random forest. Geomorphology, 391, 107889.

Hidalgo, C. A., Vega, J. A., Parra Obando, M., 2017. Effect of the Rainfall Infiltration Processes on the Landslide Hazard Assessment of Unsaturated Soils in Tropical Mountainous Regions. In T. H. II, & P. Rao (Eds.), Engineering and Mathematical Topics in Rainfall. IntechOpen. https://doi.org/ 10.5772/intechopen.70821.

Ho, K. K. S., and Ko, F. W. Y., 2009. Application of quantified risk analysis in landslide risk management practice: Hong Kong experience. Georisk, 3(3), 134-146.

Hong, H., Pradhan, B., Xu, C., Bui, D. T., 2015. Spatial prediction of landslide hazard at the Yihuang area (China) using two-class kernel logistic regression, alternating decision tree and support vector machines. Catena, 133, 266-281.

Huang, F., Chen, J., Du, Z., Yao, C., Huang, J., Jiang, Q., ..., Li, S., 2020. Landslide susceptibility prediction considering regional soil erosion based on machine-learning models. ISPRS International Journal of Geo-Information, 9(6), 377.

Huang, F., Chen, J., Liu, W., Huang, J., Hong, H., and Chen, W., 2022. Regional rainfall-induced landslide hazard warning based on landslide susceptibility mapping and a critical rainfall threshold. Geomorphology, 408, 108236.

Huang, G., Zheng, M., Peng, J., 2021. Effect of Vegetation Roots on the Threshold of Slope Instability Induced by Rainfall and Runoff. Geofluids.

Huang, Y., Zhao, L., 2018. Review on landslide susceptibility mapping using support vector machines. Catena, 165, 520-529.

Ju, N., Huang, J., He, C., Van Asch, T. W. J., Huang, R., Fan, X., ... , Wang, J. (2020). Landslide early warning, case studies from Southwest China. Engineering Geology, 279, 105917.

Kabani, A., El-Sakka, M. R., 2016, July. Object detection and localization using deep

https://doi.org/10.5194/nhess-2023-73
Preprint. Discussion started: 8 June 2023

convolutional networks with softmax activation and multi-class log loss. In International Conference on Image Analysis and Recognition (pp. 358-366). Springer, Cham.

Kadavi, P. R., Lee, C. W., Lee, S., 2019. Landslide-susceptibility mapping in Gangwon-do, South Korea, using logistic regression and decision tree models. Environmental Earth Sciences, 78(4), 1-17.

Kainthura P. and Sharma N., 2022. Machine learning driven landslide susceptibility prediction for the Uttarkashi region of Uttarakhand in India. Georisk: Assessment and Managem

Kim, J. C., Lee, S., Jung, H. S., Lee, S., 2018. Landslide susceptibility mapping using random forest and boosted tree models in Pyeong-Chang, Korea. Geocarto international, 33(9), 1000-1015.

Kim, J., Lee, K., Jeong, S., & Kim, G., 2014. GIS-based prediction method of landslide susceptibility using a rainfall infiltration-groundwater flow model. Engineering geology, 182, 63-78.

Klose, M., Maurischat, P., Damm, B., 2016. Landslide impacts in Germany: A historical and socioeconomic perspective. Landslides, 13(1), 183-199.

Kockelman, W. J., 1986. Some techniques for reducing landslide hazards. Bulletin of the Association of Engineering Geologists, 23(1), 29-52.

Lacroix, P., Handwerger, A. L., Bièvre, G., 2020. Life and death of slow-moving landslides. Nature Reviews Earth & Environment, 1(8), 404-419.

Lechner, M., Okasa, G., 2020. orf: Ordered Random Forests. R package version 0.1, 3.

Lee, S. G., Winter, M. G., 2019. The effects of debris flow in the Republic of Korea and some issues for successful risk reduction. Engineering Geology, 251, 172-189.

Lee, S. W., Kim, G. H., Yune, C. Y., Ryu, H. J., Hong, S. J., 2012. Development of landslide-risk prediction model thorough database construction. Journal of the Korean geotechnical society, 28(4), 23-33.

https://doi.org/10.5194/nhess-2023-73
Preprint. Discussion started: 8 June 2023

Lee, S. W., Kim, G., Yune, C. Y., Ryu, H. J., 2013. Development of landslide-risk assessment model for mountainous regions in eastern Korea. Disaster advances, 6(6), 70-79.

Lee, S., Hong, S. M., Jung, H. S., 2017. A support vector machine for landslide susceptibility mapping in Gangwon Province, Korea. Sustainability, 9(1), 48.

Lee, S., Lee, M. J., Jung, H. S., Lee, S., 2020. Landslide susceptibility mapping using Naïve Bayes and Bayesian network models in Umyeonsan, Korea. Geocarto international, 35(15), 1665-1679.

Li, Z., Liu, P., Wang, W., Xu, C., 2012. Using support vector machine models for crash injury severity analysis. Accident Analysis & Prevention, 45, 478-486.

Lin, L., Lin, Q., & Wang, Y. (2017). Landslide susceptibility mapping on a global scale using the method of logistic regression. Natural Hazards and Earth System Sciences, 17(8), 1411-1424.

Liu, G., Dai E., Xu, X., Wu, W., Xiang A., 2018. Quantitative Assessment of Regional Debris-Flow Risk: A Case Study in Southwest China. Sustainability, 10, 2223. https://doi.org/10.3390/su10072223

Liu, Y., Xu, C., Huang, B., Ren, X., Liu, C., Hu, B., Chen, Z., 2020. Landslide displacement prediction based on multi-source data fusion and sensitivity states. Engineering Geology, 271, 105608.

Liu, Z., Gilbert, G., Cepeda, J. M., Lysdahl, A. O. K., Piciullo, L., Hefre, H., Lacasse, S., 2021. Modeling of shallow landslides with machine learning algorithms. Geoscience Frontiers, 12(1), 385-393.

Lombardo, L., & Mai, P. M. (2018). Presenting logistic regression-based landslide susceptibility results. Engineering geology, 244, 14-24.

Louviere, J. J., Hensher, D. A., Swait, J. D., 2000. Stated choice methods: analysis and applications. Cambridge university press.

Marjanović, M., Kovačević, M., Bajat, B., Voženílek, V., 2011. Landslide susceptibility assessment using SVM machine learning algorithm. Engineering Geology, 123(3), 225-234.

Martinez-Taboada, F., Redondo, J. I., 2020. Variable importance plot (mean decrease accuracy and mean decrease Gini). Plos One, 15(4), e0230799.

Max K., 2022. caret: Classification and Regression Training. R package version 6.0-92. https://CRAN.R-project.org/package=caret.

Mayer, R., Plank, C., Bohner, A., Kollarits, S., Corsini, A., Ronchetti, F., ... and Jindra, P., 2008. Monitor: Hazard monitoring for risk assessment and risk communication. Georisk, 2(4), 195-222.

McColl, S. T., 2022. Landslide causes and triggers. In Landslide Hazards, Risks, and Disasters (pp. 13-41). Elsevier.

McCullagh, P., 1980. Regression models for ordinal data. Journal of the Royal Statistical Society: Series B (Methodological), 42(2), 109-127

McNulty, K., 2021. Handbook of Regression Modeling in People Analytics: With Examples in R and Python. Chapman and Hall/CRC.

Meena, S. R., Ghorbanzadeh, O., van Westen, C. J., Nachappa, T. G., Blaschke, T., Singh, R. P., Sarkar, R., 2021. Rapid mapping of landslides in the Western Ghats (India) triggered by 2018 extreme monsoon rainfall using a deep learning approach. Landslides, 18(5), 1937-1950.

Meena, S. R., Puliero, S., Bhuyan, K., Floris, M., Catani, F., 2022. Assessing the importance of conditioning factor selection in landslide susceptibility for the province of Belluno (region of Veneto, northeastern Italy). Natural hazards and earth system sciences, 22(4), 1395-1417.

Meyer, D., Dimitriadou, E., Hornik, K., Weingessel, A., Leisch, F., 2021. e1071: Misc

Functions of the Department of Statistics, Probability Theory Group (Formerly: E1071), TU Wien. R package version 1.7-9, https://CRAN.R-project.org/package=e1071

Nandi A.and Shakoor, A., 2008. Application of logistic regression model for slope instability prediction in Cuyahoga River Watershed, Ohio, USA. Georisk, 2(1), 16-27.

Negi, H. S., Kumar, A., Rao, N. N., Thakur, N. K., Shekhar, M. S., 2020. Susceptibility assessment of rainfall-induced debris flow zones in Ladakh–Nubra region, Indian Himalaya. Journal of Earth System Science, 129(1), 1-20.

NGII, 2018. Digital elevation model, NGII (National Geographical Information Institute), the Ministry of Land, Infrastructure and Transport, Korea.

Ngo, P. T. T., Panahi, M., Khosravi, K., Ghorbanzadeh, O., Kariminejad, N., Cerda, A., Lee, S., 2021. Evaluation of deep learning algorithms for national scale landslide susceptibility mapping of Iran. Geoscience Frontiers, 12(2), 505-519.

Noble, W. S., 2006. What is a support vector machine? Nature Biotechnology, 24(12), 1565-1567.

Ozioko, O. H., Igwe, O., 2020. GIS-based landslide susceptibility mapping using heuristic and bivariate statistical methods for Iva Valley and environs of Southeast Nigeria. Environmental monitoring and assessment, 192(2), 1-19.

Panahi, M., Gayen, A., Pourghasemi, H. R., Rezaie, F., Lee, S., 2020. Spatial prediction of landslide susceptibility using hybrid support vector regression (SVR) and the adaptive neuro-fuzzy inference system (ANFIS) with various metaheuristic algorithms. Science of the Total Environment, 741, 139937.

Park, S., Choi, C., Kim, B., Kim, J., 2013. Landslide susceptibility mapping using frequency ratio, analytic hierarchy process, logistic regression, and artificial neural network methods at the Inje area, Korea. Environmental earth sciences, 68(5), 1443-1464.

Park, S., Kim, J., 2019. Landslide susceptibility mapping based on random forest and boosted

https://doi.org/10.5194/nhess-2023-73
Preprint. Discussion started: 8 June 2023

regression tree models, and a comparison of their performance. Applied Sciences, 9(5), 942.

Peruccacci, S., Brunetti, M. T., Gariano, S. L., Melillo, M., Rossi, M., & Guzzetti, F., 2017. Rainfall thresholds for possible landslide occurrence in Italy. Geomorphology, 290, 39-57.

Pham, B. T., Tien Bui, D., Prakash, I., 2018. Bagging-based support vector machines for spatial prediction of landslides. Environmental Earth Sciences, 77(4), 1-17.

Polemio, M., and Petrucci, O. 2000. Rainfall as a landslide triggering factor an overview of recent international research. Landslides in research, theory and practice.

Popescu, M. E. 2002. Landslide causal factors and landslide remediatial options. In 3rd international conference on landslides, slope stability and safety of infra-structures (pp. 61-81). CI-Premier PTE LTD Singapore.

Rahman, H. A. A., Wah, Y. B., Huat, O. S., 2021. Predictive Performance of Logistic Regression for Imbalanced Data with Categorical Covariate. Pertanika Journal of Science & Technology, 29(1).

Rahardjo, H., Nistor, M. M., Gofar, N., Satyanaga, A., Xiaosheng, Q., and Chui Yee, S. I., 2020. Spatial distribution, variation and trend of five-day antecedent rainfall in Singapore. Georisk: Assessment and Management of Risk for Engineered Systems and Geohazards, 14(3), 177-191.

Raja, N. B., Çiçek, I., Türkoğlu, N., Aydin, O., Kawasaki, A., 2017. Landslide susceptibility mapping of the Sera River Basin using the logistic regression model. Natural Hazards, 85(3), 1323-1346.

Rengers, F. K., McGuire, L. A., Oakley, N. S., Kean, J. W., Staley, D. M., and Tang, H. ,2020. Landslides after wildfire: Initiation, magnitude, and mobility. Landslides, 17(11), 2631-2641.

Rivas, V., Remondo, J., Bonachea, J., & Sánchez-Espeso, J. (2022). Rainfall and weather conditions inducing intense landslide activity in northern Spain (Deba, Guipúzcoa). Physical Geography, 43(4), 419-439.

Sameen, M. I., Pradhan, B., Lee, S., 2020. Application of convolutional neural networks featuring Bayesian optimization for landslide susceptibility assessment. Catena, 186, 104249.

Sarkar, R., Dikshit, A., Hazarika, H., Yamada, K., Subba, K., 2019. Probabilistic rainfall thresholds for landslide occurrences in Bhutan. International Journal of Recent Technology and Engineering.

Sarkar, R., Dorji, K., 2019. Determination of the probabilities of landslide events—a case study of Bhutan. Hydrology, 6(2), 52.

Segoni, S., Piciullo, L., Gariano, S. L., 2018. A review of the recent literature on rainfall thresholds for landslide occurrence. Landslides, 15(8), 1483-1501

Shahabi, H., Hashim, M., 2015. Landslide susceptibility mapping using GIS-based statistical models and Remote sensing data in the tropical environment. Scientific reports, 5(1), 1-15.

Šilhán, K.; and Stoffel, M., 2015. Impacts of age-dependent tree sensitivity and dating approaches on dendrogeomorphic time series of landslides. Geomorphology, 236, 34-43.

Su, C., Wang, B., Lv, Y., Zhang, M., Peng, D., Bate, B.,and Zhang, S. 2022. Improved landslide susceptibility mapping using unsupervised and supervised collaborative machine learning models. Georisk: Assessment and Management of Risk for Engineered Systems and Geohazards, 1-19.

Sun, D., Xu, J., Wen, H., and Wang, D., 2021. Assessment of landslide susceptibility mapping based on Bayesian hyperparameter optimization: A comparison between logistic

https://doi.org/10.5194/nhess-2023-73
Preprint. Discussion started: 8 June 2023

regression and random forest. Engineering Geology, 281, 105972.

Sun, D., Wen, H., Wang, D., and Xu, J. 2020. A random forest model of landslide susceptibility mapping based on hyperparameter optimization using Bayes algorithm. Geomorphology, 362, 107201.

Susmaga, R., 2004. Confusion matrix visualization. In Intelligent information processing and web mining (pp. 107-116). Springer, Berlin, Heidelberg.

Takara, K., Yamashiki, Y., Sassa, K., Ibrahim, A. B., & Fukuoka, H., 2010. A distributed hydrological–geotechnical model using satellite-derived rainfall estimates for shallow landslide prediction system at a catchment scale. Landslides, 7(3), 237-258.

Tang, D., Li, D. Q., and Cao, Z. J., 2017. Slope stability analysis in the Three Gorges Reservoir Area considering effect of antecedent rainfall. Georisk: Assessment and Management of Risk for Engineered Systems and Geohazards, 11(2), 161-172.

Taylor, F. E., Tarolli, P., Malamud, B. D., 2020. Preface: Landslide–transport network interactions. Natural Hazards and Earth System Sciences, 20(10), 2585-2590.

Team, R. C., 2021. R: A language and environment for statistical computing. R Foundation for Statistical Computing, Vienna, Austria. URL https://www.R-project.org/

Tiwari, B., Ajmera, B., Gonzalez, A., and Sonbol, H. 2020. Impact of wildfire on triggering mudslides—a case study of 2018 Montecito debris flows. In Geo-Congress 2020: Engineering, Monitoring, and Management of Geotechnical Infrastructure (pp. 40-49). Reston, VA: American Society of Civil Engineers.

Turner, A. K., 2018. Social and environmental impacts of landslides. Innovative Infrastructure Solutions, 3(1), 1-25.

Vahedifard, F., Sehat, S., and Aanstoos, J. V. 2017. Effects of rainfall, geomorphological and geometrical variables on vulnerability of the lower Mississippi River levee system to slump slides. Georisk: Assessment and Management of Risk for Engineered Systems and Geohazards, 11(3), 257-271.

Van der Beek, P., 2021. Stressed rocks cause big landslides. Nature Geoscience, 14(5), 261-262.

Van Tien, P., Luong, L. H., Duc, D. M., Trinh, P. T., Quynh, D. T., Lan, N. C.,..., Loi, D. H., 2021. Rainfall-induced catastrophic landslide in Quang Tri Province: the deadliest single landslide event in Vietnam in 2020.

Wang, X., Xiao, Y., Shi, W., Ren, J., Liang, F., Lu, J., ..., Yu, X., 2022b. Forensic analysis and numerical simulation of a catastrophic landslide of dissolved and fractured rock slope subject to underground mining. Landslides, 19(5), 1045-1067.

Wang, Y., Tang, H., Huang, J., Wen, T., Ma, J., Zhang, J., 2022a. A comparative study of different machine learning methods for reservoir landslide displacement prediction. Engineering Geology, 298, 106544.

Wickham, H., François, R., Henry, L., Müller, K., 2022. dplyr: A Grammar of Data Manipulation. R package version 1.0.9, https://CRAN.R-project.org/package=dplyr

Wickham, H., 2016. ggplot2: Elegant Graphics for Data Analysis. Springer-Verlag New York.

Winter, M. G., 2020. Debris flows. Geological Society, London, Engineering Geology Special Publications, 29(1), 163-185.

Woo, C., Kwon, H., Lee, C., Kim, K., 2014. Landslide hazard prediction map based on logistic regression model for applying in the whole country of South Korea. Journal of the Korean Society of Hazard Mitigation, 14(6), 117-123.

Yesilnacar, E., and Topal, T. A. M. E. R., 2005. Landslide susceptibility mapping: a comparison of logistic regression and neural networks methods in a medium scale study, Hendek region (Turkey). Engineering Geology, 79(3-4), 251-266.

Yilmaz, I., 2009. Landslide susceptibility mapping using frequency ratio, logistic regression, artificial neural networks and their comparison: a case study from Kat landslides

https://doi.org/10.5194/nhess-2023-73
Preprint. Discussion started: 8 June 2023

Natural Hazards and Earth System Sciences
Discussions

(Tokat—Turkey). Computers & Geosciences, 35(6), 1125-1138.

Zeng, H., Tang, C. S., Zhu, C., Vahedifard, F., Cheng, Q., Shi, B., 2022. Desiccation cracking of soil subjected to different environmental relative humidity conditions. Engineering Geology, 297, 106536.

Zhao, Y., Wang, R., Jiang, Y., Liu, H., Wei, Z., 2019. GIS-based logistic regression for rainfall-induced landslide susceptibility mapping under different grid sizes in Yueqing, Southeastern China. Engineering Geology, 259, 105147.

Zhu, H., and Zhang, L. 2019. Root-soil-water hydrological interaction and its impact on slope stability. Georisk: Assessment and Management of Risk for Engineered Systems and Geohazards, 13(4), 349-359.